

Article

Integration Design and Operation Strategy of Multi-Energy Hybrid System Including Renewable Energies, Batteries and Hydrogen

Yi Zhang ^{1,2}, Hexu Sun ^{1,3,*} and Yingjun Guo ³

¹ School of Artificial Intelligence, Hebei University of Technology, Tianjin 300130, China; yzhang@hebust.edu.cn

² School of Information Science and Engineering, Hebei University of Science and Technology, Shijiazhuang 050018, China

³ School of Electrical Engineering, Hebei University of Science and Technology, Shijiazhuang 050018, China; mjl@hebust.edu.cn

* Correspondence: sunshine@hebust.edu.cn

Received: 12 September 2020; Accepted: 15 October 2020; Published: 19 October 2020



Abstract: In some areas, the problem of wind and solar power curtailment is prominent. Hydrogen energy has the advantage of high storage density and a long storage time. Multi-energy hybrid systems including renewable energies, batteries and hydrogen are designed to solve this problem. In order to reduce the power loss of the converter, an AC-DC hybrid bus is proposed. A multi-energy experiment platform is established including a wind turbine, photovoltaic panels, a battery, an electrolyzer, a hydrogen storage tank, a fuel cell and a load. The working characteristics of each subsystem are tested and analyzed. The multi-energy operation strategy is based on state monitoring and designed to enhance hydrogen utilization, energy efficiency and reliability of the system. The hydrogen production is guaranteed preferentially and the load is reliably supplied. The system states are monitored, such as the state of charge (SOC) and the hydrogen storage level. The rated and ramp powers of the battery and fuel cell and the pressure limit of the hydrogen storage tank are set as safety constraints. Eight different operation scenarios comprehensively evaluate the system's performance, and via physical experiments the proposed operation strategy of the multi-energy system is verified as effective and stable.

Keywords: multi-energy complementation; operation strategy; state monitoring; AC-DC hybrid bus; hydrogen energy subsystem; experiment platform

1. Introduction

In recent years, wind and solar power generation have rapidly developed. However, due to the fluctuation of wind/solar energy and the insufficient capacity of transmission lines, the problem of abandoning renewable energy is very serious. Thus, large amounts of clean energy and social investment have been wasted, and this has remarkably affected the process of upgrading energy structures [1–3].

The most effective way to solve the problem of renewable energy absorption is to efficiently convert, store and reuse surplus electrical energy. Electrical energy can be converted into hydrogen for storage by means of electrolyzing water. Hydrogen is supplied to fuel cell buses or chemical industries. Due to the diverse applications of hydrogen energy subsystems, renewable energy penetration rates can be increased and pollutant emissions can be reduced. In this way, the reliability and stability of power supplies can be improved [4–7].

An energy network including wind power and hydrogen subsystems has been established by the E.ON company in Germany wherein hydrogen is produced at $360 \text{ Nm}^3/\text{h}$, and the rated power of wind turbines is 2MW and hydrogen is added into the natural gas pipeline at a volume ratio of 2%. Thus, the conversion and storage of wind energy is realized. In Norway, a micro-grid was built that included wind turbines, electrolyzers and a fuel cell. In windy weather, wind turbines directly provided electricity for families, with surplus electricity used to produce hydrogen. Then, the hydrogen was compressed and stored in the tank. In the absence of wind, the fuel cell is engaged to produce the necessary electricity. The electricity demand of residents is therefore guaranteed. Hydrogen energy is also widely used in hybrid tramways, peak loads and the frequency regulation of power grids [8–12]. In [13], a transportation system was researched that included a fuel cell as its main energy source. A reduced-order model of the system was proposed by a differential flatness algorithm.

Research on multi-energy complementary systems is still in its early stages. The key technical issues have focused on coupling mechanisms, optimal control and energy management of the hybrid system integrating wind turbines, photovoltaic panels, batteries, electrolyzers and fuel cells [14–17]. However, the energy utilization efficiency and economy of the system needs to be further improved [18–21].

In [22–26], optimization schemes based on fuzzy inference and online learning are proposed, and simulations of the energy system carried out. As a result the power quality of the grid-connected system was improved. In [27–30], due to the intermittence and uncertainty of the renewable energy, different architectures of direct current (DC) transmission lines and hydrogen storage subsystems are proposed to reduce the adverse impact of power fluctuations on the power grid and improve renewable energy utilization. In [31–34], hybrid systems including renewable energy and hydrogen energy are modeled, simulated and analyzed. The dispatching schemes based on model prediction control improved the system efficiency. In [35–37], hydrogen energy subsystems are designed to effectively supplement and regulate renewable energy, considering the obvious seasonal characteristics of local wind and solar resources. In [38–40], solar power and hydrogen production systems are studied. Due to the intermittence of solar energy, batteries are introduced along with controllers designed to supervise the whole system. In [41–44], an economic analysis of a comprehensive system is carried out, and optimal scheduling schemes of the system are put forward. In [45–47], the application of a hydrogen energy subsystem is researched in order to suppress power fluctuations. The system's operational costs and efficiencies are optimized through coordination control. The feasibility of the system is also studied. In [48–51], wind and photovoltaic power as main power sources are discussed, with an application scenario of residential power supply. Models based on integer linear programming are proposed, and the capacity allocation method is analyzed. In [52–55], a model of a multi-energy system is constructed, with operation characteristics analyzed in their off-grid applications. In [56,57], a hybrid system is proposed based on renewable energy and a fuel cell. Photovoltaic panels and wind turbines are modeled as the power flow, with load-following control regulating the system. The fuel economy was ultimately improved by switching strategies in the whole load range.

The structure of a multi-energy system is complex. The relevant literature has proposed single AC bus architecture that requires were many additional converters, and the corresponding energy loss reduces system efficiency. These references studied both off-grid and grid-connected systems integrating multiple energy sources such as wind turbines, photovoltaic panels, batteries, electrolyzers and fuel cells. However, these studies have mainly been based on power systems, with hydrogen energy subsystems utilized only as a supplement to participate in peak load shifting—the efficient production of hydrogen has never been the primary objective of the system. As hydrogen energy has been underutilized, its advantages have not typically been well exploited, including its high calorific value and clean energy. The random fluctuations of renewable energy and loads have made system operations more complicated, and this has also been affected by the state of charge and hydrogen storage levels. In these references, the operation scenarios of the systems are relatively simple, and the uncertainty of the entire system is not given enough consideration. Whether previous studies have

used characteristic tests of each unit in the system (e.g., the fuel cell) or tested the operation strategies of the overall system based on software simulations, there has been very little research into building a physical platform for experimentation.

The contributions of the multi-energy integrated system and operation strategy proposed in this paper are summarized as follows.

- (1) This paper presents a hybrid AC/DC bus structure utilizing a photovoltaic panel, battery and fuel cell that all generate DC power, with a DC load in the system. The distributed generation and load can be directly connected to the DC bus. Thus, the converters are reduced and the efficiency of the multi-energy integrated system is improved. Although an AC/DC hybrid structure has been mentioned in some studies, previous devices have still worked using AC power, and remained connected to an AC bus. Therefore, they have only been connected to a DC bus by a converter.
- (2) The objective of the system's operation is to ensure sufficient hydrogen output and a reliable power supply. The main role of the hydrogen energy subsystem is not to provide supplementary energy for the regulating power system. Hydrogen is directly transported to the hydrogen station through the pipeline to the fuel cell bus. In addition, hydrogen is added to the natural gas pipeline at a certain ratio as a mixed fuel.
- (3) Due to the uncertainty of renewable energy and the fluctuations of loads, a control method based on an expert strategy is proposed and verified using multiple scenarios. The working states are monitored for the operation strategy, such as the state of charge and the hydrogen storage level. The eight operation scenarios fully reflect the randomness of the entire system.
- (4) The physical equipment platform of a multi-energy system is built that contains a wind turbine, photovoltaic panel, PEM electrolyzer, PEM fuel cell, hydrogen storage tank, battery, load and central controller. The working characteristic of each unit is tested, such as the fuel cell. The effectiveness of the operation strategy is verified by means of a physical platform rather than the software simulation.

2. Architecture of Multi-Energy Integrated System

The topology of the multi-energy integrated system is shown in Figure 1, including the wind turbine, photovoltaic panel, hydrogen energy subsystem, battery and load. The black line in Figure 1 represents the power flow. The red line indicates the information flow, and the blue line shows the hydrogen flow. The red boxes represent the central and local controllers.

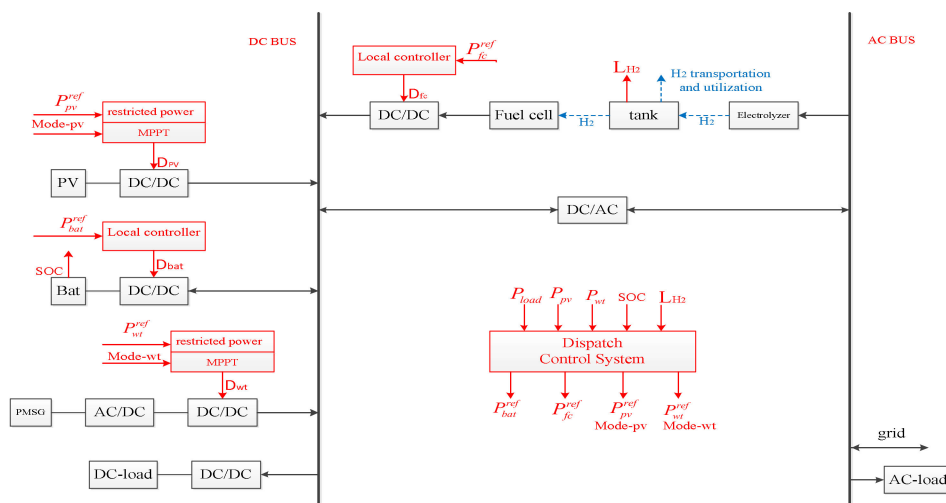


Figure 1. Topology of multi-energy integrated system.

The photovoltaic panel operated in maximum power point tracking (MPPT) or restricted power mode. The adaptive fuzzy control algorithm is designed to utilize the maximum solar energy. The photovoltaic system is required to operate in the restricted power mode at the power reference value, which is set by the scheduling instruction of the central controller. The photovoltaic panel is connected to a DC bus via a DC/DC converter.

A three-blade wind turbine was used in this experiment. The permanent magnet synchronous generator (PMSG) operates in MPPT (maximum power point tracking) or restricted power mode. The improved climbing search method was designed for utilizing the maximum wind energy. The wind turbine is required to operate in the restricted power mode at the power reference value, which is set by the scheduling instruction of the central controller. The wind turbine is connected to the DC bus via AC/DC and DC/DC devices.

The battery is connected to the DC bus via a bi-directional DC/DC converter. When the energy of the whole system is surplus, the battery is used to store the excess net energy. Otherwise, the battery is utilized to supply the deficient energy to the load. The state of charge (SOC) of the battery is transmitted to the central controller. The output power of the battery follows the power reference value.

The DC load is connected to the DC bus by via a DC/DC converter. The DC bus of the system is connected to the AC bus via a bidirectional DC/AC device.

The AC bus is connected to the grid by a point of common coupling (PCC). The AC load is connected to the AC bus. When the energy of the integrated system is deficient, an external power grid is able to provide necessary support.

The electrolyzer unit is connected to the AC bus and operates at the rated power. The high purity hydrogen is produced and stored in the metal hydride storage tank as the solid state, which significantly improves the safety and stability of the hydrogen energy subsystem. The storage level of the hydrogen tank is transmitted to the central controller. This hydrogen can be directly used in fuel cell vehicles and chemical industry applications, while the remaining hydrogen is supplied to the fuel cell in the integrated system in order to satisfy electricity demand. The fuel cell is connected to the DC bus via a DC/DC converter. The output power of the fuel cell is adjusted by the central controller.

These converters are regulated throughout the entire system by their respective local controllers. The pulse width modulation (PWM) signals with controllable duty cycles are generated according to the scheduling instructions. The central controller monitors the operation state of the equipment. The power reference values of these modules in the multi-energy integrated system are determined by means of the operation strategy.

The capacity configurations of multi-energy integrated platforms according to load demand and system economy are shown in the Table 1. The manufacturers of these units are also listed in the Table 1.

Table 1. Capacity configurations of multi-energy complementary systems.

Unit	Manufacturer	Parameters
Photovoltaic panel	Axitec AC-250P×4	1 KW
Wind turbine	Primus Wind Power Air 30	0.4 KW
Wind turbine	Wind speed (cut in)	3 m/s
Wind turbine	Wind speed (cut off)	12.5 m/s
Wind turbine	Wind speed (max)	49 m/s
Hydrogen storage tan	Ovonic Model 85G250B-NPT×3	10 bar,500 sl per tank
PEMFC	Heliocentris Nexa 1200	1.2 KW
PEMFC	Max current	60 A
PEMFC	Output voltage	20–36 VDC
PEM electrolyzer	Schmidlin NM-H2 PLUS	0.4 KW
Lead acid battery	Banner Stand-by Bull SBV 12-55×4	55 AH

The integrated system equipment is shown in Figure 2. The left cabinet is the hydrogen energy subsystem, which includes an electrolyzer, a hydrogen storage tank, a fuel cell, and a safety device for monitoring hydrogen leakage. The right cabinet is the power subsystem. It includes a battery, a load, converters, and a controller. The middle part is the switch cabinet. It includes a relay, a transducer, and a data acquisition and network communication module.



Figure 2. Integrated system equipment.

The structure of the multi-energy integrated system is shown in Figure 3. The black line represents the power flow. The red line indicates the information flow, and the blue line shows the hydrogen flow. A two-level control scheme is designed in the integrated energy system. According to the system state and operation strategy, the central controller sends the decision command to the local controllers. Modbus TCP/IP protocol is used for communication.

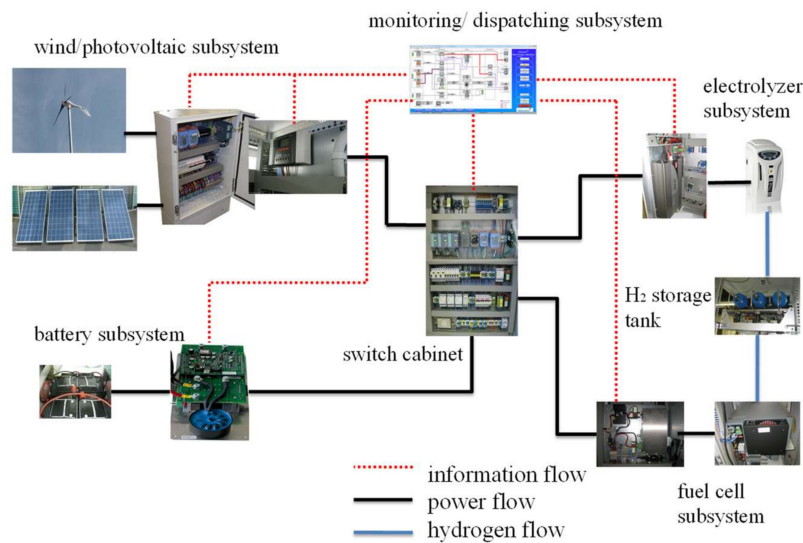


Figure 3. Multi-energy system structure.

3. Unit Characteristics of the Multi-Energy System

3.1. Wind Turbine

A permanent magnet synchronous generator (PMSG) is used in the experiment. The wind turbine is directly coupled with the synchronous generator, replacing a heavy speed-increasing gear box. The controllable converter is applied in the generator unit. PMSGs have many advantages, such as high efficiency and reliability, minimal maintenance, and a low operation cost [58]. The power captured by the wind turbine can be expressed as the following formula:

$$P = \frac{1}{2} C_P(\lambda, \beta) A \rho v^3 \quad (1)$$

where P is the output power, ρ is the air density (1.225 kg/m^3), A is the area swept by the wind turbine, v is the wind speed, and C_P is the wind energy utilization coefficient, which is related to the pitch angle (β) and tip speed ratio (λ).

The pitch angle control is adopted to achieve the most efficient operation. The maximum power point tracking (MPPT) algorithm is based on power feedback and a climbing search [59]. The characteristic curve of wind speed output power is shown in Figure 4, which depicts the physical experiment.

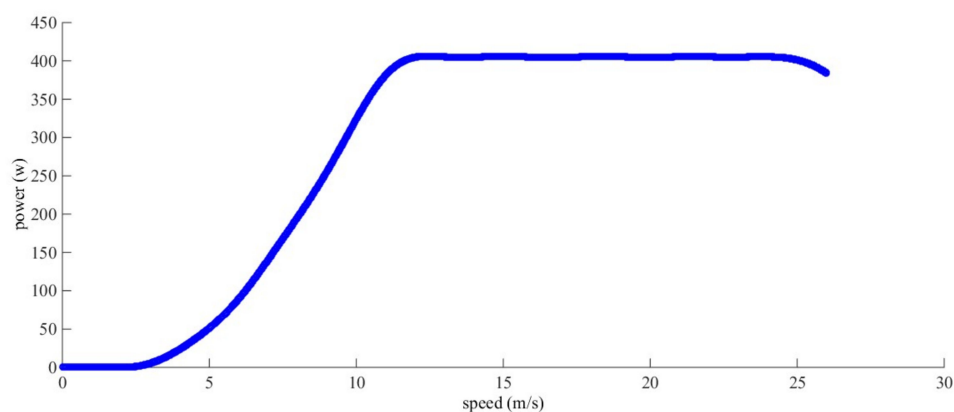


Figure 4. Wind speed-output power curve.

3.2. Photovoltaic Panel

The equivalent circuit of the photovoltaic cell is shown in Figure 5 [60]. The I-V characteristic varies with solar radiation intensity and temperature. The corresponding equation is expressed as follows:

$$I = I_{ph} - I_{sat} \left\{ \exp \left[\frac{q(V + I \cdot R_s)}{A \cdot K \cdot T} \right] - 1 \right\} - \frac{V + I \cdot R_s}{R_{sh}} \quad (2)$$

where I_{ph} is the photocurrent, I_{sat} is the diode reverse saturation current, R_s is the series equivalent resistance, R_{sh} is the parallel equivalent resistance, A is the diode factor, K is the Boltzmann constant (1.38×10^{-23} J/K), q is the electron charge (1.6×10^{-19} C), T is the absolute temperature of the photovoltaic cell, V is the output voltage, and I is the output current.

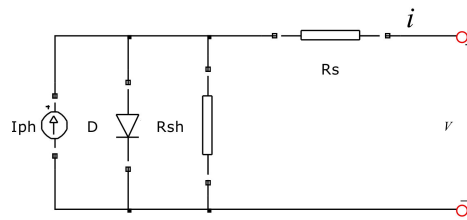


Figure 5. Equivalent circuit of the photovoltaic cell.

Commonly used parameters in engineering include open circuit voltage V_{oc} , short circuit current i_{sc} , maximum power point voltage V_m , and maximum power point current I_m . These parameters are obtained under standard testing conditions (i.e., $S_{ref} = 1000$ W/m², $T_{ref} = 25$ °C) [61]. The following are assumed: (1) The effect of the parallel equivalent resistance R_{sh} is ignored; (2) because the series equivalent resistance is less than the forward resistance of the diode, the approximate expression is described as $I_{ph} \approx I_{sc}$.

Thus, the I-V characteristic equation is simplified as follows:

$$I = I_{sc} \left\{ 1 - C_1 \left[\exp \left(\frac{V}{C_2 V_{oc}} \right) - 1 \right] \right\} \quad C_1 = \left(1 - \frac{I_m}{I_{sc}} \right) \exp \left(-\frac{V_m}{C_2 V_{oc}} \right) \quad C_2 = \left(\frac{V_m}{V_{oc}} - 1 \right) \frac{1}{\ln(1 - I_m/I_{sc})} \quad (3)$$

where C_1 and C_2 are determined by the commonly used engineering parameters.

When the solar radiation intensity and cell temperature do not meet the standard conditions, the I-V characteristics are modified according to the following formulas:

$$\Delta T = T - T_{ref} \quad \Delta I = \alpha(S/S_{ref})\Delta T + (S/S_{ref} - 1)I_{sc} \quad \Delta V = -\beta\Delta T - R_s\Delta I \quad (4)$$

where α and β are the current-temperature coefficient and voltage-temperature coefficient, respectively [62].

The I-V and P-V characteristic curves of the photovoltaic cell are shown in the Figure 6, and were obtained by the physical experiment. As the temperature rises, the open circuit voltage decreases and the short circuit current increases. Correspondingly, the maximum power point voltage and current all decrease. The MPPT strategy is based on the conductance increment and fuzzy logic [60].

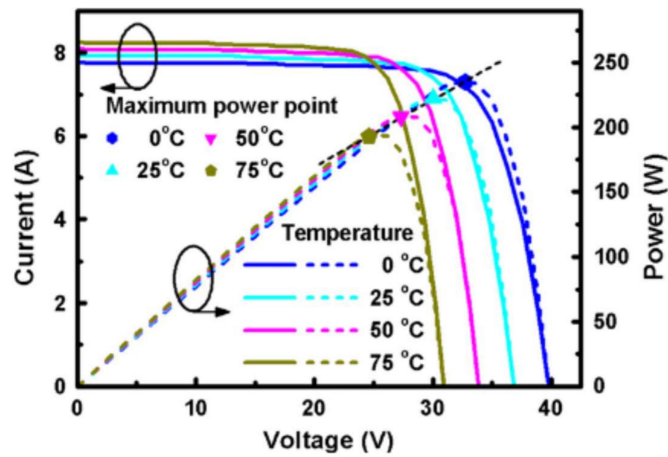
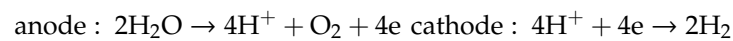


Figure 6. I-V and P-V characteristic curves of the photovoltaic panel.

3.3. PEM Electrolyzer

The strong electrolyte is not needed in the proton exchange membrane (PEM) electrolyzer. Because of the combined action of the electric field and the porous platinum catalyst, hydrated ions (H_3O^+) can directly reach the cathode through the proton exchange membrane [63]. Thus, hydrogen is generated at the cathode. The reaction equations are as follows:



The electrical characteristic of the electrolyzer is as follows:

$$U = U_{\text{rev}} + \frac{\alpha}{A} I_{\text{el}} + \beta \log\left(\frac{\gamma}{A} I_{\text{el}} + 1\right) \quad (5)$$

where U is the working voltage, I_{el} is the working current, A is the electrode area, U_{rev} is the reversible voltage (1.23 V), and α , β , γ are all experimental parameters.

The expression for the hydrogen production rate is as follows:

$$m_{\text{H}_2} = \eta \frac{I_{\text{el}}}{2F} \quad (6)$$

where F is the Faraday constant (96485C/mol), and η is the efficiency of the electrolyzer. The working characteristic curve of the PEM electrolyzer is shown in Figure 7.

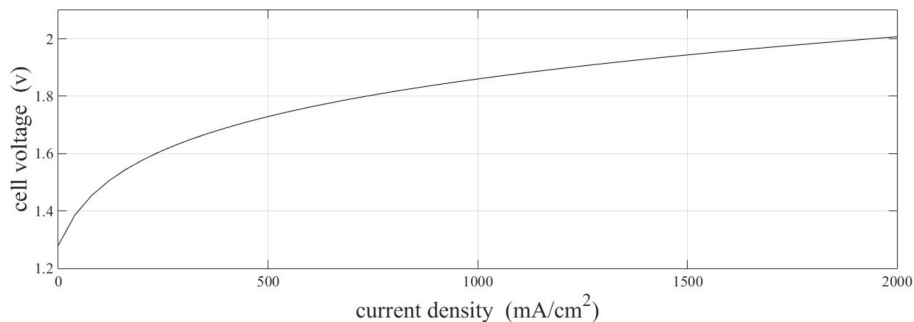
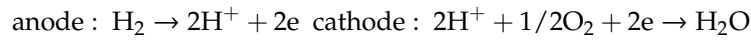


Figure 7. Characteristic curve of the electrolyzer.

3.4. PEM Fuel Cell

In the proton exchange membrane (PEM) fuel cell, hydrogen fuel oxidizes at the anode and the oxidant undergoes a reduction reaction at the cathode. Both poles contain catalysts to accelerate the

electrode reaction. The proton exchange membrane only allows H^+ to pass, while the electrons lost from H_2 are transmitted through the external wire. The PEM fuel cell is equivalent to the DC power source [64]. The reaction equations are as follows:



The working voltage is described as follows:

$$U = E_N - U_{act} - U_{ohm} - U_{con} \quad (7)$$

where E_N is actually the open circuit voltage, U_{act} is the activation voltage drop, U_{ohm} is the ohmic voltage drop, and U_{con} is the concentration voltage drop.

Hydrogen consumption can be calculated by the following formula:

$$m_{H_2\text{use}} = 2m_{O_2\text{use}} = \frac{I_{FC}}{2F} \quad (8)$$

where I_{FC} is the working current of the PEM fuel cell, and F is the Faraday constant. The working characteristic curve of the PEM fuel cell is shown in Figure 8. The blue line represents the relationship between the fuel cell current and hydrogen consumption. The red line represents the relationship between the current and the voltage of the fuel cell. As the output current of the fuel cell increases, hydrogen consumption increases linearly and the voltage slightly decreases.

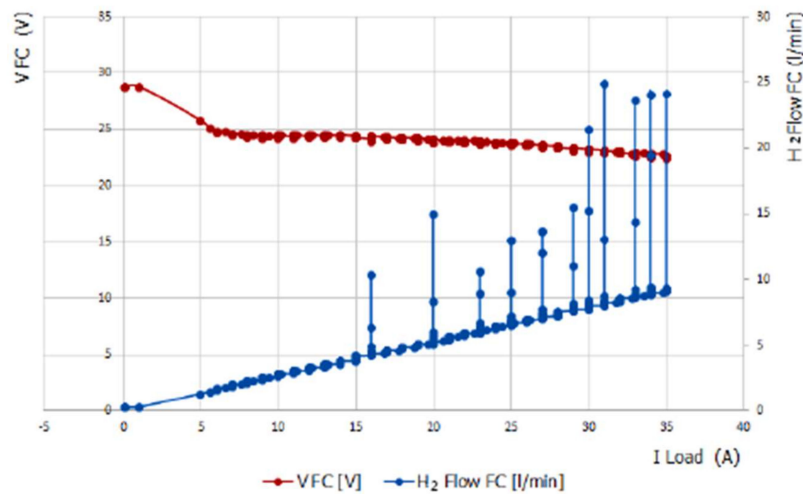


Figure 8. Characteristic curve of PEM fuel cell.

3.5. Battery

The battery model consists of a controlled voltage source and series resistance. The controlled voltage source is based on the actual state of charge [65]. The non-linear equation is as follows:

$$E = E_0 - \gamma \frac{Q}{Q - \int idt} + A \exp\left(-B \cdot \int idt\right) \quad (9)$$

where E is the no-load voltage, E_0 is the constant battery voltage, γ is the polarization voltage, A is the amplitude of the exponential zone, B is the reciprocal of the time constant of exponential zone, and Q is battery capacity.

The terminal voltage of battery is expressed as follows:

$$V_{bat} = E - Ri \quad (10)$$

where R is the series resistance of the battery. The working characteristic curve of battery is shown in Figure 9. The figure shows the relationship between the battery voltage and discharge time at different discharge currents. As the discharge current decreases, the discharge time increases and the attenuation of battery voltage slows down.

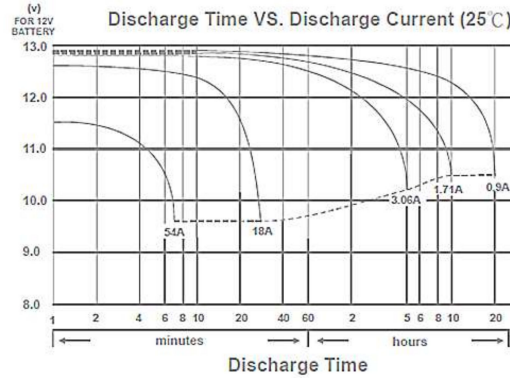


Figure 9. Characteristic curve of the battery.

4. System Operation Strategy

4.1. Performance Indicator

There are many modules involved in a multi-energy complementary system, such as wind turbines, photovoltaic panels, hydrogen energy subsystems, batteries, and the load. In order to improve the utilization of renewable resources (wind and solar power) and the hydrogen storage level, it is necessary to propose an operation strategy to coordinate the integrated system. The energy efficiency of the entire system and the loss of load probability (LLP) also need to be considered comprehensively.

The utilization ratio of renewable energy (URRE) is expressed as follows:

$$URRE = 1 - \frac{\int_0^T P_{\text{curtail}}(t) dt}{\int_0^T P_{\text{renew}}(t) dt} \quad (11)$$

where $P_{\text{curtail}}(t)$ is the curtailed power of renewable resources (wind and solar power), and $P_{\text{renew}}(t)$ is the maximum available power of renewable resources.

The hydrogen storage level (HSL) is calculated as follows:

$$HSL = \frac{\int_0^T L_{H_2}(t) dt}{T} \quad (12)$$

where $L_{H_2}(t)$ is the real-time state of the hydrogen storage tank.

The energy efficiency of the integrated system is described as follows:

$$\eta = \frac{\int_0^T P_{\text{load}}(t) dt}{\int_0^T P_{\text{renew}}(t) dt + E_{H_2} \int_0^T M_{H_2}(t) dt + \int_0^T P_{\text{bat}}(t) dt} \quad (13)$$

where $P_{\text{load}}(t)$ is the load power, $M_{H_2}(t)$ is the hydrogen consumption rate, E_{H_2} is the calorific value of hydrogen, and $P_{\text{bat}}(t)$ is the battery power.

The loss of load probability is calculated as follows:

$$LLP = \frac{\int_0^T LPS(t) dt}{\int_0^T P_{\text{load}}(t) dt} \quad (14)$$

where $LPS(t)$ is the loss of the power supply.

4.2. System Optimization Function

Optimization functions are proposed for the multi-energy system as follows:

- (1) In order to meet the hydrogen demand of fuel cell buses and other industries, sufficient hydrogen production must be ensured. Thus, a high hydrogen storage level needs to be maintained, and the corresponding optimization function is as follows:

$$\min \left\{ 1 - \frac{\int_0^T L_{H_2}(t) dt}{T} \right\} \quad (15)$$

- (2) Energy loss occurs during the “electricity–hydrogen–electricity” conversion process in the fuel cell and electrolyzer equipment. In addition, energy loss also occurs in the battery’s charging and discharging processes. Thus, high efficiency of the system needs to be met, and the corresponding optimization function is as follows:

$$\min \left\{ 1 - \frac{\int_0^T P_{load}(t) dt}{\int_0^T P_{renew}(t) dt + E_{H_2} \int_0^T M_{H_2}(t) dt + \int_0^T P_{bat}(t) dt} \right\} \quad (16)$$

- (3) In order to improve the reliability of system’s power supply, loss of load probability needs to be reduced. The corresponding optimization function is as follows:

$$\min \left\{ \frac{\int_0^T LPS(t) dt}{\int_0^T P_{load}(t) dt} \right\} \quad (17)$$

- (4) Wind and photovoltaic power should be used to a maximum extent. Thus, it is necessary to curtail reductions of wind and photovoltaic power while improving the penetration rate of renewable energy. The corresponding optimization function is as follows:

$$\min \left\{ \frac{\int_0^T P_{curtail}(t) dt}{\int_0^T P_{renew}(t) dt} \right\} \quad (18)$$

4.3. System Optimization Method

There are four optimization objectives of the system’s operation, and system efficiency, the reliability of a power supply and the penetration rate of renewable energy are all comprehensively considered. Furthermore, the hydrogen storage level is given priority among system objectives, as compared with the traditional operation of a power system. Some of these objectives are in conflict. Moreover, the working conditions are complex and changeable due to the randomness and uncertainty of renewable energy systems. Figure 10 displays the proposed expert strategy for the system’s operation based on different states in the experiment.

The hydrogen storage level is judged first. If the hydrogen is insufficient, the electrolyzer is opened to produce hydrogen. Otherwise, the electrolyzer is not started. Afterwards, it is judged whether or not there is surplus renewable energy. If there is surplus energy and the state of charge of the battery is not full, the battery is charged, preferably. If the battery is fully charged, the surplus power is sent to the grid (depending to the grid connection requirement); otherwise, the renewable energy is deemed insufficient. If the state of charge is not empty, the battery is discharged to meet the load demand. If the hydrogen storage tank is full, the fuel cell is turned on as a supplement. Thus, the reliability of the system power supply is improved. Finally, deficit power is purchased from the grid according to the grid connection requirement.

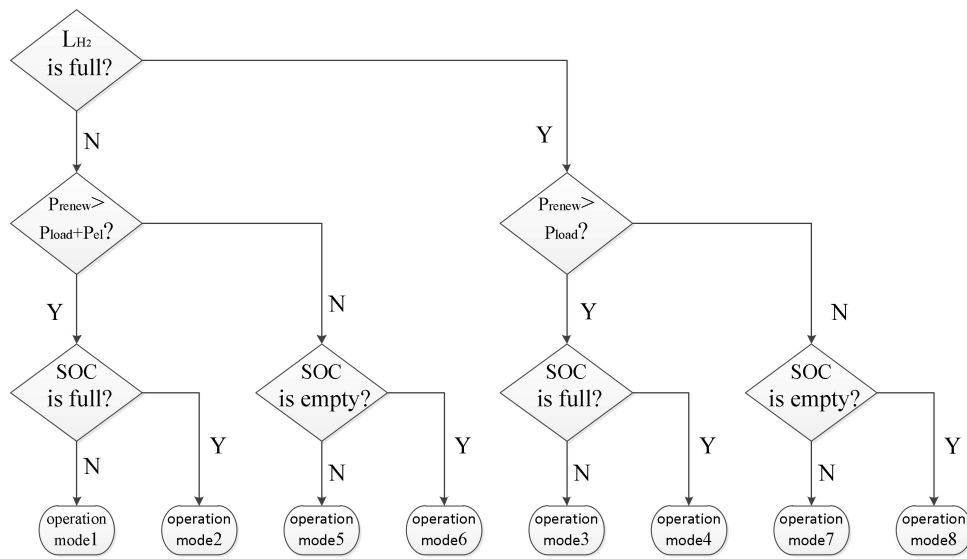


Figure 10. Operation strategy model.

Hydrogen production is considered to be the priority of the integrated system, and the pressure of the hydrogen storage tank is taken as the system safety constraint. In order to improve the safety and stability of the system and ensure the purity of hydrogen production, it is necessary to reasonably set the working state of the electrolyzer. In this system, the electrolyzer operates under constant power. The fuel cell operates under variable power, depending on the actual working conditions. The hydrogen storage level, state of charge, and load power are all monitored, along with the output power of wind turbine and photovoltaic panel. The central controller not only optimizes the start-up and shutdown of fuel cell and electrolyzer equipment, but also sets the working mode of battery, wind turbine, and photovoltaic panel. The power reference values are determined, as well as the interaction with the external power grid. These operation modes reflect the randomness and uncertainty of the entire system.

The constraints of the system operation are as follows:

- (1) The condition for starting the fuel cell is $p_{\text{tank}} \geq p_{\text{min}(fc)}$. The condition for starting the electrolyzer is $p_{\text{tank}} \leq p_{\text{max}}$, where p_{tank} is the pressure of the hydrogen storage tank, $p_{\text{min}(fc)}$ is the minimum pressure of the hydrogen storage required to maintain the start-up of the fuel cell, and p_{max} is maximum safety pressure of hydrogen storage tank.
- (2) The following condition for the fuel cell must be met: $P_{fc} \leq P_{fc(\text{rating})}$, where P_{fc} is the working power of the fuel cell and $P_{fc(\text{rating})}$ is the rated power of the fuel cell.
- (3) Power fluctuation can reduce the efficiency and purity of the hydrogen production. In order to solve the problems, the electrolyzer operates under a constant power condition (i.e., $P_{el} = P_{el(\text{rating})}$, where $P_{el(\text{rating})}$ is the rated power of the electrolyzer).

4.4. Operation Modes Analysis

The eight operation modes of the multi-energy system are described in detail as follows.

(1) Operation mode 1

If $P_{wt} + P_{pv} > P_{load} + P_{el(\text{rating})}$, L_{H_2} is not full, SOC is not full, then the power balance equation of the system is expressed as follows:

$$P_{wt} + P_{pv} = P_{load} + P_{el(\text{rating})} + P_{bat} \quad (19)$$

The wind turbine and photovoltaic panel operate in MPPT mode and the battery is charged. The fuel cell does not work, and the electrolyzer starts to produce hydrogen.

(2) Operation mode 2

If $P_{wt} + P_{pv} > P_{load} + P_{el(rating)}$, L_{H_2} is not full, SOC is full, then the power balance equation of the system is expressed in two cases as follows:

$$P_{wt} + P_{pv} = P_{load} + P_{el(rating)} + P_{grid} \quad (20)$$

In this case, the surplus energy is permitted to be delivered to the grid. The wind turbine and photovoltaic panel operate in MPPT mode. The fuel cell does not work, and the electrolyzer starts to produce hydrogen.

$$P_{wt(ref)} + P_{pv(ref)} = P_{load} + P_{el(rating)} \quad (21)$$

In this case, the surplus energy is not permitted to be delivered to the grid. The wind turbine and photovoltaic panel operate in restricted power mode. The fuel cell does not work, and the electrolyzer starts to produce hydrogen.

(3) Operation mode 3

If $P_{wt} + P_{pv} > P_{load}$, L_{H_2} is full, SOC is not full, then the power balance equation of the system is expressed as follows:

$$P_{wt} + P_{pv} = P_{load} + P_{bat}, P_{el} = 0 \quad (22)$$

The wind turbine and photovoltaic panel operate in MPPT mode and the battery is charged. The fuel cell and electrolyzer do not work.

(4) Operation mode 4

If $P_{wt} + P_{pv} > P_{load}$, L_{H_2} is full, SOC is full, then the power balance equation of the system is expressed in two cases as follows:

$$P_{wt} + P_{pv} = P_{load} + P_{grid}, P_{el} = 0 \quad (23)$$

In this case the surplus energy is permitted to be delivered to the grid. The wind turbine and photovoltaic panel operate in MPPT mode. The fuel cell and electrolyzer do not work.

$$P_{wt(ref)} + P_{pv(ref)} = P_{load}, P_{el} = 0 \quad (24)$$

In this case the surplus energy is not permitted to be delivered to the grid. The wind turbine and photovoltaic panel operate in restricted power mode. The fuel cell and electrolyzer do not work.

(5) Operation mode 5

If $P_{wt} + P_{pv} < P_{load} + P_{el(rating)}$, L_{H_2} is not full, SOC is not empty, then the power balance equation of the system is expressed as follows:

$$P_{wt} + P_{pv} + P_{bat} = P_{load} + P_{el(rating)} \quad (25)$$

The wind turbine and photovoltaic panel operate in MPPT mode and the battery is discharged. The fuel cell does not work, and the electrolyzer starts to produce hydrogen.

(6) Operation mode 6

If $P_{wt} + P_{pv} < P_{load} + P_{el(rating)}$, L_{H_2} is not full, SOC is empty, then the power balance equation of the system is expressed as follows:

$$P_{wt} + P_{pv} + P_{grid} = P_{load} + P_{el(rating)} + P_{bat} \quad (26)$$

The wind turbine and photovoltaic panel operate in MPPT mode and the battery is charged. In order to support the multi-energy system, the system is connected to the external power grid. The fuel cell does not work, and the electrolyzer starts to produce hydrogen.

(7) Operation mode 7

If $P_{wt} + P_{pv} < P_{load}$, L_{H_2} is full, SOC is not empty, then the power balance equation of the system is expressed as follows:

$$P_{wt} + P_{pv} + P_{bat} + P_{fc} = P_{load} \quad (27)$$

The wind turbine and photovoltaic panel operate in MPPT mode and the battery is discharged. The electrolyzer does not work, and the fuel cell starts to supply the electricity.

(8) Operation mode 8

If $P_{wt} + P_{pv} < P_{load}$, L_{H_2} is full, SOC is empty, then the power balance equation of the system is expressed as follows:

$$P_{wt} + P_{pv} + P_{fc} = P_{load} + P_{bat} \quad (28)$$

The wind turbine and photovoltaic panel operate in MPPT (maximum power point tracking) mode and the battery is charged. The electrolyzer does not work, and the fuel cell starts to supply the electricity.

The operation states of the integrated system are summarized in Table 2.

Table 2. Summary of operation states.

Mode	Power Equation	Renewables	Electrolyzer	H2 Tank	Fuel Cell	Battery	Grid
1	Equation (19)	MPPT	ON	not full	OFF	not full/charge	OFF
2	Equation (20)	MPPT	ON	not full	OFF	full/OFF	ON/sell
	Equation (21)	restricted power	ON	not full	OFF	full/OFF	OFF
3	Equation (22)	MPPT	OFF	full	OFF	not full/charge	OFF
4	Equation (23)	MPPT	OFF	full	OFF	full/OFF	ON/sell
	Equation (24)	restricted power	OFF	full	OFF	full/OFF	OFF
5	Equation (25)	MPPT	ON	not full	OFF	not empty/discharge	OFF
6	Equation (26)	MPPT	ON	not full	OFF	empty/charge	ON/buy
7	Equation (27)	MPPT	OFF	full	ON	not empty/discharge	OFF
8	Equation (28)	MPPT	OFF	full	ON	empty/charge	OFF

5. Experiment Result and Analysis

The entire system integrates a wind turbine, photovoltaic panel, battery, and hydrogen subsystem. The working scenarios of the system are complex and changeable. The fluctuations of wind and solar power are violent. The load power is uncertain. The central coordination controller can make the system efficient and steady [66]. The hydrogen production is preferentially guaranteed. The load power is reliably supplied. Detailed experiment results are discussed below, according to the different states of source–load–storage. Each scenario corresponds to the same mode studied in the operation strategy.

5.1. Scenario 1

Wind and solar energy are sufficient. In addition, the hydrogen storage level and state of charge are not full. Wind and solar power provide a stable supply for the load. The electrolyzer starts to produce hydrogen, and the excess energy is stored in the battery.

As shown in Figure 11, the intensity of solar radiation is high, and the solar power is about 900 W. The solar power varies with the radiation intensity. The peak power of wind turbine is 392 W, and its randomness is obviously stronger than the solar power. The load power piecewise increases from 100 to 420 W. In order to improve the purity of hydrogen production and prolong the device's life, the electrolyzer operates at constant power. The surplus power can be stored in the battery. The overall trend of charging power can reflect the surplus energy of the system. When the load power is large, the charging power is small, and vice versa.

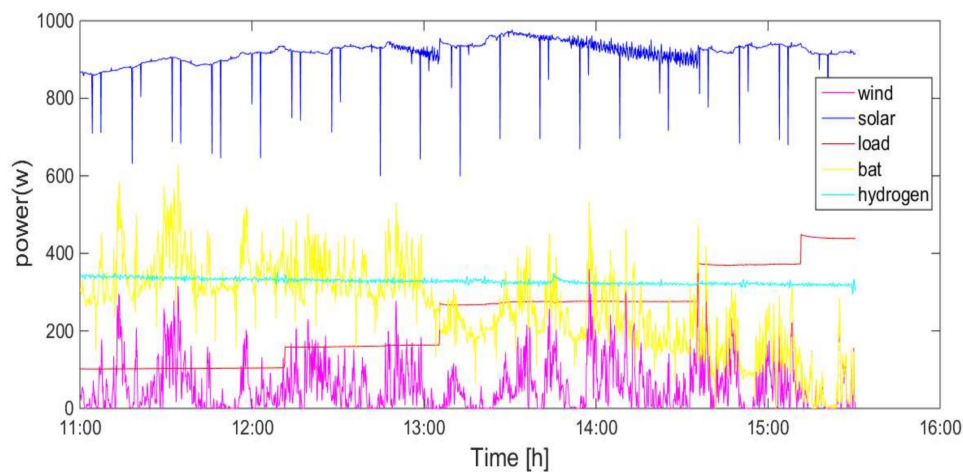


Figure 11. Power curves in scenario 1.

The hydrogen storage level and the state of charge are shown in Figure 12. The intensity of solar radiation slightly fluctuates from 770 to 830 W/m². The wind speed sharply varies, showing obvious inherent uncertainty that sometimes is lower than the cut-in wind speed, and sometimes reaches the rated wind speed. The hydrogen production flow is relatively stable, at 0.8 sl/min. The pressure of hydrogen storage tank linearly increases from 3.8 to 4.5 bar. Meanwhile the state of charge increases from 36% to 54%.

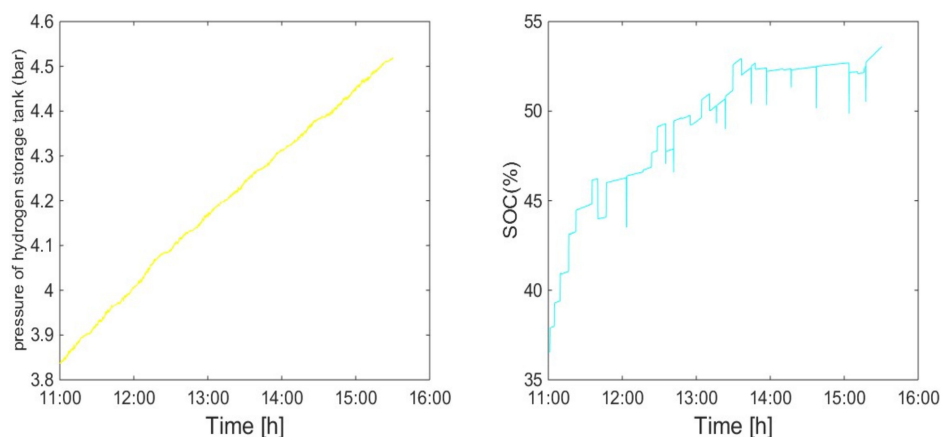


Figure 12. Operation state curves in scenario 1.

5.2. Scenario 2

Wind and solar energy are sufficient. In addition, the hydrogen storage level is not full, but the state of charge is full. Wind and solar power can stably supply the load. The electrolyzer starts to produce hydrogen. The excess energy is delivered to the grid or directly discarded, as shown in Figures 13 and 14, respectively.

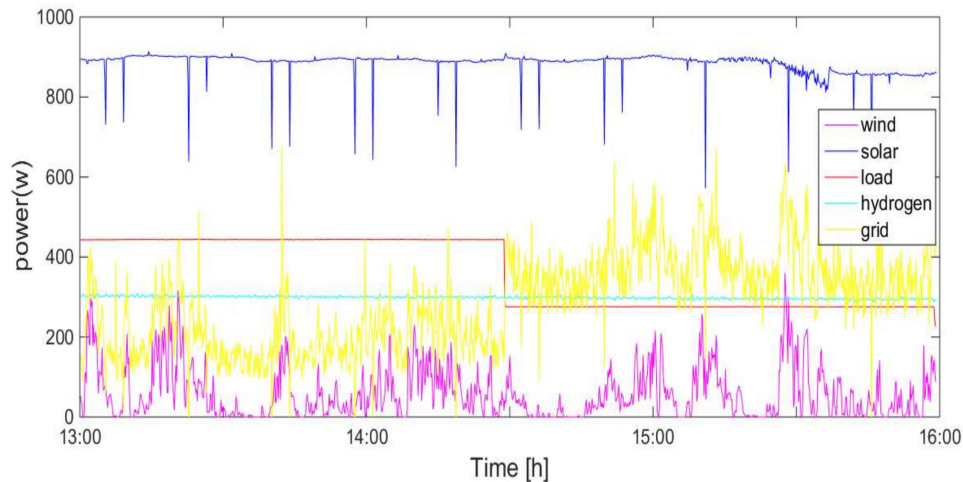


Figure 13. Power curves in scenario 2 (grid-connected).

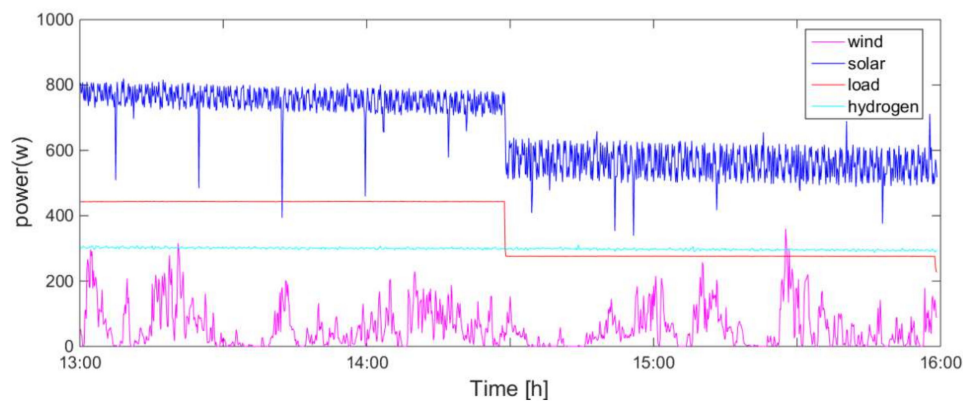


Figure 14. Power curves in scenario 2 (restricted power).

The maximum solar power reaches 900 W. The load power falls from 450 to 280 W. The wind power is intermittent and fluctuant, and the electrolyzer operates in constant power. When the grid-connected condition is met, the system delivers surplus energy to the grid, as shown in Figure 13.

When the grid-connected condition is not met, the system operates in restricted power mode. During this period, the excess of renewable energy is not absorbed, as shown in Figure 14.

5.3. Scenario 3

Wind and solar energy are sufficient. In addition, the hydrogen storage level is full, but the state of charge is not full. Wind and solar power can stably supply the load. The excess energy is stored in the battery, as shown in Figure 15. The electrolyzer is shut down. Solar power output slightly fluctuates, and the load power non-monotonically varies.

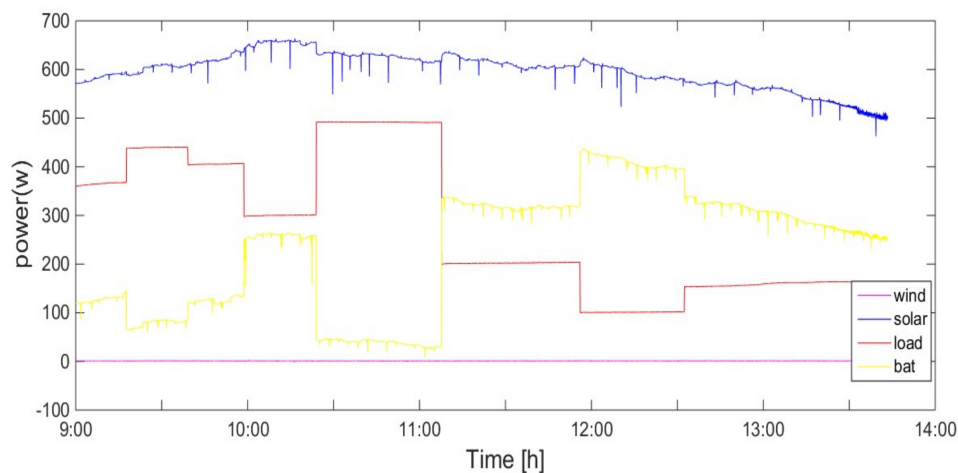


Figure 15. Power curves in scenario 3.

5.4. Scenario 4

The wind and solar energy are sufficient. In addition, the hydrogen storage level and state of charge are full. Wind and solar power can stably supply the load. The surplus energy is delivered to the grid or directly discarded.

The electrolyzer is not started. When the grid-connected condition is met, the system delivers the surplus energy to the grid. The photovoltaic panel works in MPPT mode. The solar power is about 600 W with small fluctuations. The load power also shows a strong change, which is always less than the renewable energy. When the load power is small, the power delivered to the grid is large, and vice versa.

When the grid-connected condition is not met, the system operates under restricted power. The excess of renewable energy is not absorbed, as shown in Figure 16.

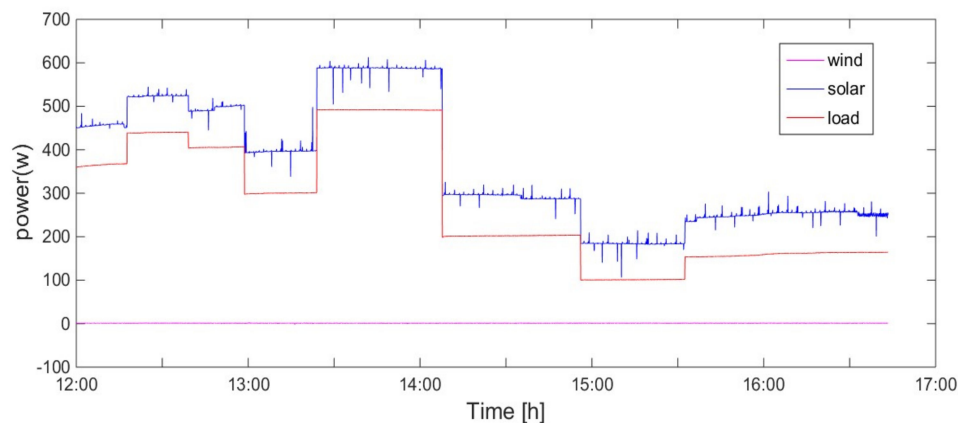


Figure 16. Power curves in scenario 4 (restricted power).

5.5. Scenario 5

Wind and solar energy are insufficient. The hydrogen storage level is not full and the state of charge is not empty. This operation period is at night. The photovoltaic panel does not work. The wind speed is less than the cut-in wind speed. The load power increases from 95 to 230 W. The battery discharges to ensure stable hydrogen production and an uninterrupted supply for the load, as shown in Figure 17.

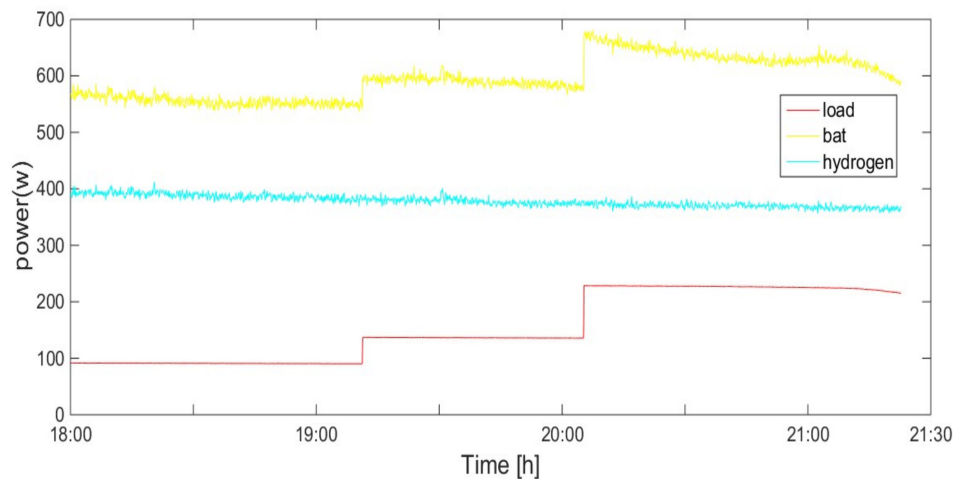


Figure 17. Power curves in scenario 5.

The hydrogen storage level and state of charge are shown in Figure 18. The intensity of solar radiation fluctuates slightly from 60 to 55 W/m². The wind speed varies sharply, showing obvious inherent uncertainty, but the wind speed is lower than the cut-in speed. The hydrogen flow is relatively stable, at a value of 0.83 sl/min. The state of charge drops from 87% to 39%. The pressure of the hydrogen storage tank linearly increases from 2.8 to 3.5 bar.

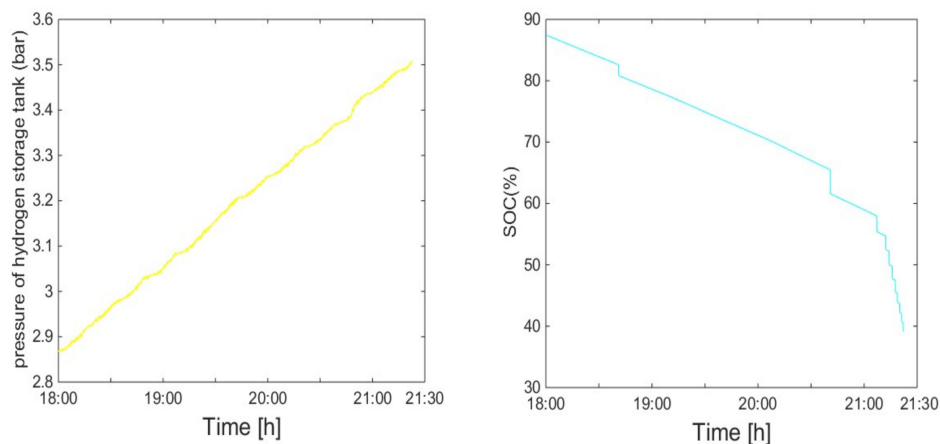


Figure 18. Operation state curves in scenario 5.

5.6. Scenario 6

Wind and solar energy are insufficient. The hydrogen storage level is not full and the state of charge is empty. In order to ensure stable hydrogen production and an uninterrupted supply for the load, the system needs to be connected to the grid, as shown in Figure 19. The working period is cloudy, and the wind speed is lower than the cut-in wind speed. Solar power is low, and slowly increases from 220 to 300 W. The load power varies and is higher than the renewable energy. The power from the grid is about 710 W. In addition to supplying power to the load, the external grid also provides constant power for the electrolyzer and charges the battery. When the load power is high, the charging power is low, and vice versa.

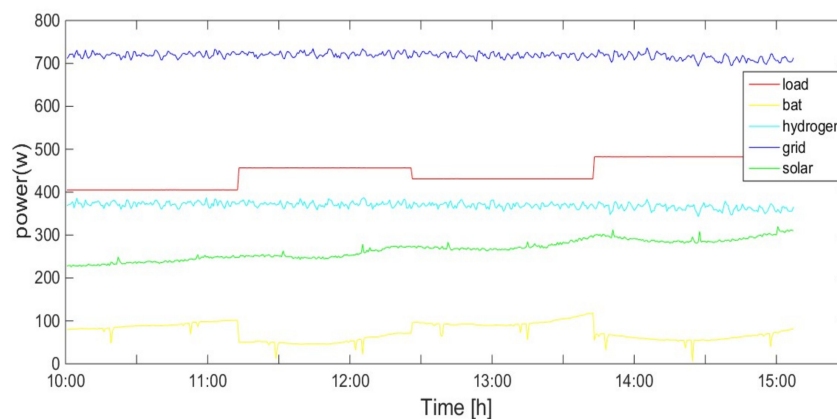


Figure 19. Power curves in scenario 6.

5.7. Scenario 7

Wind and solar energy are insufficient. The hydrogen storage level is full and the state of charge is not empty. When the deficit power of the load is small, the battery independently operates in the discharged state to ensure that the uninterrupted working of the load. Meanwhile, the fuel cell does not work, as shown in Figure 20. Solar power rises from 260 to 480 W, but is weaker than the load power, with an irregular change.

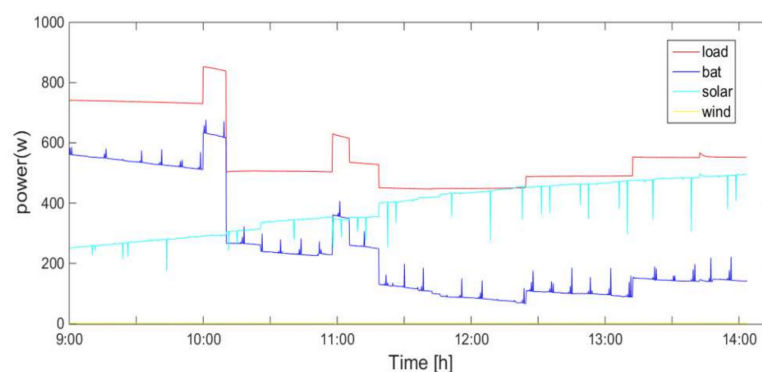


Figure 20. Power curves in scenario 7 (without the fuel cell).

When the deficit power of the load is large, the battery and fuel cell all work to continuously supply the load, as shown in Figure 21. The intensity of the solar radiation is weak, at only 50 W, and the load power changes from 1100 to 1350 W. The output power of the fuel cell is 1 kW, but this is not enough to meet the load demand. The battery is discharged for its uninterrupted power supply. The trend of the battery output power is consistent with that of the load power.

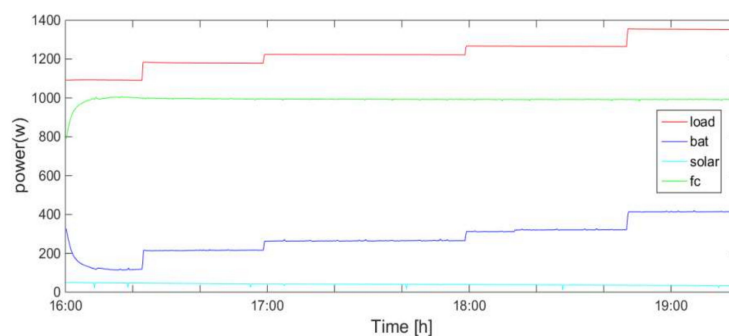


Figure 21. Power curves in scenario 7 (with the fuel cell).

The pressure of the hydrogen storage tank and the state of charge are shown in Figure 22. In order to maintain reliable operation of the fuel cell, the hydrogen flow stabilizes at 14.5 sl/min. The pressure of the hydrogen storage tank decreases from 4.4 to 1.1 bar. The state of charge decreases from 81% to 57%.

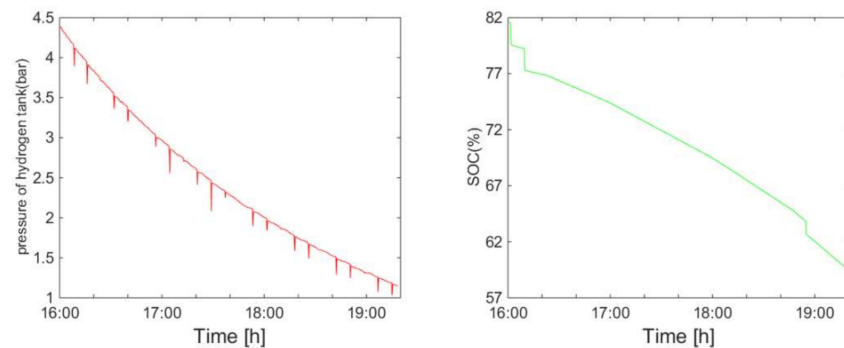


Figure 22. Operation state curves in scenario 7 (with the fuel cell).

5.8. Scenario 8

Wind and solar energy are insufficient. The hydrogen storage level is full and the state of charge is empty. The fuel cell works to supply the load and charge the battery, as shown in Figure 23. The working period is at night. Solar power is zero, and the wind speed is less than the cut-in wind speed.

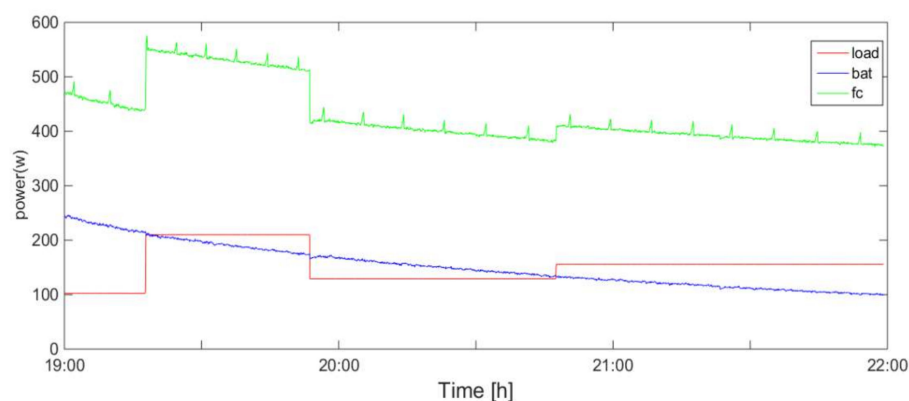


Figure 23. Power curves in scenario 8.

The pressure of the hydrogen storage tank and the state of charge are shown in Figure 24. The trend of hydrogen flow is consistent with that of the output power of the fuel cell. The pressure of the hydrogen storage tank decreases from 3.6 to 1.4 bar. The state of charge increases from 20% to 47%.

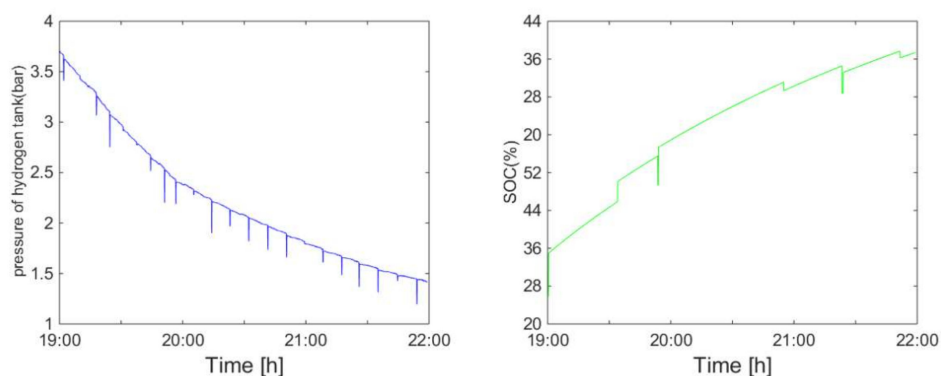


Figure 24. Operation state curves in scenario 8.

5.9. Performance Analysis

The experiment results described in Equations (11)–(14) are shown in Table 3. The results of [19] are also listed in the Table 3 as a baseline. The utilization ratio of renewable energy is about 91.2%. The integrated system contains two kinds of energy storage units, namely, batteries and a hydrogen energy subsystem, allowing more renewable energy to be stored, transformed, and utilized. Due to the high penetration rate of renewable energy, the problem of wind and solar power curtailment is partly solved, with a hydrogen storage level of about 71.4%. Due to the high calorific value of hydrogen, the integrated system prioritizes hydrogen production, which is supplied to the chemical and transportation industries. Hydrogen is supplied to the fuel cell in order to meet the load demand only when renewable energy and storage batteries are insufficient under the off-grid working condition; therefore, the hydrogen storage level is high. The efficiency of the integrated system is about 70.2%, with energy loss occurring in converters, batteries, and the electricity-hydrogen subsystem. Because the system adopts an AC/DC hybrid bus structure, the converters in the system are reduced, and the fuel cell is only turned on under limited operation conditions. As a result, the overall energy efficiency is high, with a loss of load probability of about 7.3%. There are hybrid energy storage units in the system, but when renewable energy and hybrid energy storage are both insufficient, load loss occurs under the off-grid working condition. The loss of load probability is higher than that of the corresponding reference. There is contradiction between the URRE and LLP. With increases in system configuration capacity, loss of load probability decreases; however, wind and solar power curtailment increase, which reduces the utilization ratio of renewable energy. The loss of load probability in the reference is low, while the utilization ratio of renewable energy is not mentioned.

Table 3. Summary of experiment results.

Performance Indicators	This Paper	Reference [19]	Traditional Method
utilization ratio of renewable energy (URRE)	91.2%	not mentioned	91.2%
hydrogen storage level (HSL)	71.4%	54.4%	51.3%
efficiency of the integrated system (η)	70.2%	56.6%	80.6%
loss of load probability (LLP)	7.3%	1.68%	6.1%

The traditional operation strategy of the system is shown in Figure 25 as a baseline. This operation strategy is based on the battery as the central regulator of the system. As an auxiliary means, the hydrogen energy subsystem only plays the role of electric energy conversion. The corresponding system performance is also shown in Table 3. The electricity–hydrogen–electricity conversion process is greatly decreased; therefore, the energy loss is reduced and the operation efficiency of the system is significantly improved. However, the hydrogen storage level is correspondingly reduced because hydrogen production is not the main objective in this case. The loss of load probability is slightly reduced.

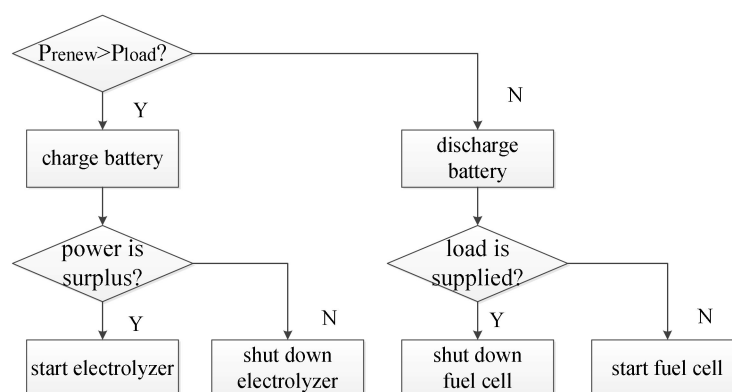


Figure 25. Traditional operation method.

6. Conclusions

A multi-energy complementary system is designed in this paper. Because the photovoltaic panel, battery, and fuel cell all generate DC power and there is a DC load in the system, an AC/DC hybrid bus structure is presented. The distributed power generation and load can be directly connected to the DC bus. Thus, the converters are reduced and the efficiency of the multi-energy system is improved.

The objective of system operation is to ensure stable hydrogen output and a reliable power supply. The main role of the hydrogen energy subsystem does not act as supplementary energy for regulating the power system, and the hydrogen production of the multi-energy system is increased.

Due to the uncertainty of renewable energy and the fluctuation of the load, an operation strategy based on state monitoring was proposed and verified in various scenarios. These application scenarios can fully reflect the randomness of the entire system.

A physical equipment platform was built for the multi-energy system containing a wind turbine generator, photovoltaic panel, PEM electrolyzer, PEM fuel cell, hydrogen storage tank, battery, load, and central controller. The working characteristics of each unit and the proposed operation strategy were tested by means of the physical platform rather than a software simulation. Wind and solar power curtailment was reduced and hydrogen storage was increased.

Author Contributions: Author contributions: Writing—review and editing, methodology, formal analysis, Y.Z.; project administration, supervision, funding acquisition, H.S.; data curation, Y.G. All authors have read and agreed to the published version of the manuscript.

Funding: This research was funded by the National Natural Science Foundation of China (61472273); Civil-Military Integration Innovation Foundation of Shijiazhuang Science and Technology Bureau (191130164A); Key Project of Hebei Science and Technology Department (20314501D, 19214501D); Foreign intelligence introduction project of Hebei Science and Technology Department (2019YX005A).

Conflicts of Interest: The authors declare no conflict of interest.

References

1. Esa, P.; Hannele, H.; Tiina, K. Path toward 100% renewable energy future and feasibility of power-to-gas technology in Nordic countries. *IET Renew. Power Gener.* **2017**, *11*, 1695–1706.
2. Md, S.A.; Seyed, A. Energy Management in Power Distribution Systems: Review, Classification, Limitations and Challenges. *IEEE Access* **2019**, *7*, 92979–93001.
3. Rahbar, K.; Chai, C.C.; Zhang, R. Energy Cooperation Optimization in Microgrids with Renewable Energy Integration. *IEEE Trans. Smart Grid* **2018**, *9*, 1482–1493. [[CrossRef](#)]
4. Mendis, N.; Muttaqi, K. An Effective Power Management Strategy for a Wind–Diesel–Hydrogen-Based Remote Area Power Supply System to Meet Fluctuating Demands under Generation Uncertainty. *IEEE Trans. Ind. Appl.* **2015**, *51*, 1228–1238. [[CrossRef](#)]
5. Luis, V.; Felipe, R.; Carlos, B. Planning and Management of a Hydrogen-Based Microgrid. *IEEE Trans. Ind. Inform.* **2013**, *9*, 1398–1404.
6. Raúl, S.; Luis, M. Electrolyzer models for hydrogen production from wind energy systems. *Int. J. Hydrogen Energy* **2015**, *40*, 2927–2938.
7. Pablo, G.; Juan, P. Improving long-term operation of power sources in off-grid hybrid systems based on renewable energy, hydrogen and battery. *J. Power Sources* **2014**, *265*, 149–159.
8. Pablo, G.; Luis, M. Energy Management System of Fuel-Cell-Battery Hybrid Tramway. *IEEE Trans. Ind. Electron.* **2010**, *57*, 4013–4023.
9. Ridong, Z.; Jili, T. GA-Based Fuzzy Energy Management System for FC/SC-Powered HEV Considering H2 Consumption and Load Variation. *IEEE Trans. Fuzzy Syst.* **2018**, *26*, 1833–1843.
10. Juan, P.; Pablo, G. Predictive Control for the Energy Management of a Fuel Cell Battery Supercapacitor Tramway. *IEEE Trans. Ind. Inform.* **2014**, *10*, 276–285.
11. Pablo, G.; Francisco, L.; Carlos, A. Long-term optimization based on PSO of a grid-connected renewable energy/battery/hydrogen hybrid system. *Int. J. Hydrogen Energy* **2014**, *39*, 10805–10816.
12. Wang, C.; Yang, X.; Wu, Z.; Che, Y.; Guo, L.; Zhang, S.; Liu, Y. Highly Integrated and Reconfigurable Microgrid Testbed with Hybrid Distributed Energy Sources. *IEEE Trans. Smart Grid* **2016**, *7*, 451–459. [[CrossRef](#)]

13. Phatiphat, T.; Matheepot, P. Differential Flatness Based-Control Strategy of a Two-Port Bidirectional Supercapacitor Converter for Hydrogen Mobility Applications. *Energies* **2020**, *13*, 2794.
14. Osman Haruni, A.M.; Michael Negnevitsky, M. A Novel Operation and Control Strategy for a Standalone Hybrid Renewable Power System. *IEEE Trans. Sustain. Energy* **2013**, *4*, 402–413. [[CrossRef](#)]
15. Luis, V.; Carlos, B.; Felipe, R. Integration of Fuel Cell Technologies in Renewable-Energy-Based Microgrids Optimizing Operational Costs and Durability. *IEEE Trans. Ind. Electron.* **2016**, *63*, 167–177.
16. Manuel, C.; Antonio, C. Sizing optimization, dynamic modeling and energy management strategies of a stand-alone PV/hydrogen/battery-based hybrid system. *Int. J. Hydrogen Energy* **2013**, *38*, 3830–3845.
17. Pablo, G.; Juan, P.T.; Luis, M.F. Optimal energy management system for stand-alone wind turbine/photovoltaic/hydrogen/battery hybrid system with supervisory control based on fuzzy logic. *Int. J. Hydrogen Energy* **2013**, *38*, 14146–14158.
18. Pablo, G.; Luis, M.F. Optimized operation combining costs, efficiency and lifetime of a hybrid renewable energy system with energy storage by battery and hydrogen in grid-connected applications. *Int. J. Hydrogen Energy* **2016**, *41*, 23132–23144.
19. Juan, P.T.; Pablo, G. Control based on techno-economic optimization of renewable hybrid energy system for stand-alone applications. *Expert Syst. Appl.* **2016**, *51*, 59–75.
20. Pablo, G.; Juan, P.T. Energy management system based on techno-economic optimization for microgrids. *Electr. Power Syst. Res.* **2016**, *131*, 49–59.
21. Felix, G.; Carlos, B. Optimal Economical Schedule of Hydrogen-Based Microgrids with Hybrid Storage Using Model Predictive Control. *IEEE Trans. Ind. Electron.* **2015**, *62*, 5195–5207.
22. Garcia, P.; Garcia, C. ANFIS-based control of a grid-connected hybrid system integrating renewable energies, hydrogen and batteries. *IEEE Trans. Ind. Inform.* **2014**, *10*, 1107–1117. [[CrossRef](#)]
23. Felipe, V.; Doris, S.; Jorge, C. Robust Energy Management System Based on Interval Fuzzy Models. *IEEE Trans. Control Syst. Technol.* **2016**, *24*, 140–157.
24. Felipe, V.; Jorge, C.; Doris, S. Robust Energy Management System for a Microgrid Based on a Fuzzy Prediction Interval Model. *IEEE Trans. Smart Grid* **2016**, *7*, 1486–1494.
25. Mehdi, R.; Mohsen, M.; Caisheng, W. Optimal fuzzy-based power management for real time application in a hybrid generation system. *IET Renew. Power Gener.* **2017**, *11*, 1325–1334.
26. Zhang, R.; Tao, J.; Zhou, H. Fuzzy Optimal Energy Management for Fuel Cell and Supercapacitor Systems Using Neural Network Based Driving Pattern Recognition. *IEEE Trans. Fuzzy Syst.* **2019**, *27*, 45–57. [[CrossRef](#)]
27. Melo, D.; Chang, C. Synergistic control between hydrogen storage and offshore wind farm for grid operation. *IEEE Trans. Sustain. Energy* **2014**, *5*, 18–27. [[CrossRef](#)]
28. Senjyu, T.; Nakaji, K. A hybrid power system using alternative energy facilities in isolated island. *IEEE Trans. Energy Convers.* **2005**, *20*, 406–414. [[CrossRef](#)]
29. Phatiphat, T.; Suwat, S.; Pongsiri, M. DC Bus Stabilization of Li-Ion Battery Based Energy Storage for a Hydrogen/Solar Power Plant for Autonomous Network Applications. *IEEE Trans. Ind. Appl.* **2015**, *51*, 2717–2725.
30. Katayoun, R.; Jie, X.; Rui, Z. Real-Time Energy Storage Management for Renewable Integration in Microgrid: An Off-Line Optimization Approach. *IEEE Trans. Smart Grid* **2015**, *6*, 124–134.
31. Trifkovic, M.; Sheikhzadeh, M. Modeling and control of a renewable hybrid energy system with hydrogen storage. *IEEE Trans. Control Syst. Technol.* **2014**, *22*, 169–179. [[CrossRef](#)]
32. Tao, Z.; Bruno, F. Real-Time Emulation of a Hydrogen-Production Process for Assessment of an Active Wind-Energy Conversion System. *IEEE Trans. Ind. Electron.* **2009**, *56*, 737–746.
33. Ali Pourmousavi, S.; Hashem Nehrir, M. Real-Time Energy Management of a Stand-Alone Hybrid Wind-Microturbine Energy System Using Particle Swarm Optimization. *IEEE Trans. Sustain. Energy* **2010**, *1*, 193–201. [[CrossRef](#)]
34. Lee, D.J.; Wang, L. Small-Signal Stability Analysis of an Autonomous Hybrid Renewable Energy Power Generation/Energy Storage System Part I: Time-Domain Simulations. *IEEE Trans. Energy Convers.* **2008**, *23*, 311–320. [[CrossRef](#)]
35. AhmadiS, M. Performance of a standalone wind-hydrogen power system for regions with seasonal wind profile: A case study in Khaf region. *Sustain. Energy Technol. Assess.* **2014**, *7*, 266–278.
36. Mathiesen, B.V.; Lund, H. Comparative analyses of seven technologies to facilitate the integration of fluctuating renewable energy sources. *IET Renew. Power Gener.* **2009**, *3*, 190–204. [[CrossRef](#)]

37. Juan, P.T.; Pablo, G. Energy dispatching based on predictive controller of an off-grid wind turbine/photovoltaic/hydrogen/battery hybrid system. *Renew. Energy* **2015**, *74*, 326–336.
38. Loong, Y.; Dahari, M. Development of a system configuration for a solar powered hydrogen facility using fuzzy logic control. *J. Zhejiang Univ. Sci. A Appl. Phys. Eng.* **2013**, *14*, 822–834. [[CrossRef](#)]
39. Agbossou, K.; Kolhe, M. Performance of a stand-alone renewable energy system based on energy storage as hydrogen. *IEEE Trans. Energy Convers.* **2004**, *19*, 633–640. [[CrossRef](#)]
40. Jerónimo, J.M.; Paul, F.P. Development and Implementation of a Supervisor Strategy and Sliding Mode Control Setup for Fuel-Cell-Based Hybrid Generation Systems. *IEEE Trans. Energy Convers.* **2015**, *30*, 218–225.
41. Cai, G.; Kong, L. Techno-economic analysis of wind curtailment/hydrogen production /fuel cell vehicle system with high wind penetration in china. *CSEE J. Power Energy Syst.* **2017**, *3*, 44–52. [[CrossRef](#)]
42. Brunetto, C.; Tina, G. Optimal hydrogen storage sizing for wind power plants in day ahead electricity market. *IET Renew. Power Gener.* **2007**, *1*, 220–226. [[CrossRef](#)]
43. Antonio, C.; Francisco, J.; Higinio, S. Optimal sizing of stand-alone hybrid systems based on PV/WT/FC by using several methodologies. *J. Energy Inst.* **2014**, *87*, 330–340.
44. Hamed, B.; Ramezan, A. Multi-criteria optimal sizing of hybrid renewable energy systems including wind, photovoltaic, battery, and hydrogen storage with ϵ -constraint method. *IET Renew. Power Gener.* **2018**, *12*, 883–892.
45. Takahashi, R.; Kinoshita, H. Output power smoothing and hydrogen production by using variable speed wind generators. *IEEE Trans. Ind. Electron.* **2010**, *57*, 485–493. [[CrossRef](#)]
46. Khalid, F. Analysis and assessment of an integrated hydrogen energy system. *Int. J. Hydrogen Energy* **2015**, *41*, 7960–7967. [[CrossRef](#)]
47. Wai, R.J.; Jhung, S.J.; Liaw, J.J.; Chang, Y.R. Intelligent Optimal Energy Management System for Hybrid Power Sources Including Fuel Cell and Battery. *IEEE Trans. Power Electron.* **2013**, *28*, 3231–3244. [[CrossRef](#)]
48. Won, W.; Kwon, H. Design and operation of renewable energy sources based hydrogen supply system: Technology integration and optimization. *Renew. Energy* **2017**, *103*, 226–238. [[CrossRef](#)]
49. Sungjin, L.; Beom, K. Joint Energy Management System of Electric Supply and Demand in Houses and Buildings. *IEEE Trans. Power Syst.* **2014**, *29*, 2804–2812.
50. Christopher, O.A.; Lingfeng, W. Autonomous Appliance Scheduling for Household Energy Management. *IEEE Trans. Smart Grid* **2014**, *5*, 673–682.
51. Adriana, C.; Nelson, L.D. Mixed integer Linear Programming Based Energy Management System for Hybrid PV Wind Battery Microgrids: Modeling, Design, and Experimental Verification. *IEEE Trans. Power Electron.* **2017**, *32*, 2769–2783.
52. Gao, D.; Jiang, D. An integrated energy storage system based on hydrogen storage: Process configuration and case studies with wind power. *Energy* **2014**, *66*, 332–341. [[CrossRef](#)]
53. Fan, X.; Wang, W. Hybrid pluripotent coupling system with wind and photovoltaic-hydrogen energy storage and the coal chemical industry in Hami, Xinjiang. *Renew. Sustain. Energy Rev.* **2017**, *72*, 950–960. [[CrossRef](#)]
54. Brka, A.; Kothapalli, G. Predictive power management strategies for stand-alone hydrogen systems: Lab-scale validation. *Int. J. Hydrogen Energy* **2015**, *40*, 9907–9916. [[CrossRef](#)]
55. Garcia-Trivino, P.; GilMena, A. Power control based on particle swarm optimization of grid-connected inverter for hybrid renewable energy system. *Energy Convers. Manag.* **2015**, *91*, 83–92. [[CrossRef](#)]
56. Nicu, B.; Valentin, A.S.; Angel, C.C. Optimization of the Fuel Cell Renewable Hybrid Power System Using the Control Mode of the Required Load Power on the DC Bus. *Energies* **2019**, *12*, 1889.
57. Nicu, B.; Phatiphat, T. Energy Efficiency and Fuel Economy of a Fuel Cell/Renewable Energy Sources Hybrid Power System with the Load-Following Control of the Fueling Regulators. *Mathematics* **2020**, *8*, 151.
58. Abdallah, T. Energy Management in the Decentralized Generation Systems Based on Renewable Energy—Ultracapacitors and Battery to Compensate the Wind/Load Power Fluctuations. *IEEE Trans. Ind. Appl.* **2015**, *51*, 1817–1827.
59. Zhu, Y.; Cheng, M.; Hua, W.; Wang, W. A Novel Maximum Power Point Tracking Control for Permanent Magnet Direct Drive Wind Energy Conversion Systems. *Energies* **2012**, *5*, 1398–1412. [[CrossRef](#)]
60. Zhang, Y.; Sun, H.X. Research on maximum power point tracking method of photovoltaic power generation. *J. Intell. Fuzzy Syst.* **2019**, *37*, 3149–3162. [[CrossRef](#)]
61. Qi, W.; Liu, J.; Christofides, P.D. Distributed Supervisory Predictive Control of Distributed Wind and Solar Energy Systems. *IEEE Trans. Control Syst. Technol.* **2013**, *21*, 504–512. [[CrossRef](#)]

62. Wei, Q.; Shi, G.; Song, R.; Liu, Y. Adaptive Dynamic Programming-Based Optimal Control Scheme for Energy Storage Systems with Solar Renewable Energy. *IEEE Trans. Ind. Electron.* **2017**, *64*, 5468–5478. [[CrossRef](#)]
63. Fang, R.; Liang, Y. Control strategy of electrolyzer in a wind-hydrogen system considering the constraints of switching times. *Int. J. Hydrogen Energy* **2019**, *44*, 25104–25111. [[CrossRef](#)]
64. Sun, L.; Wu, G.; Xue, Y.; Shen, J.; Li, D.; Lee, K.Y. Coordinated Control Strategies for Fuel Cell Power Plant in a Microgrid. *IEEE Trans. Energy Convers.* **2018**, *33*, 1–9. [[CrossRef](#)]
65. Shen, J.; Khaligh, A. A Supervisory Energy Management Control Strategy in a Battery/Ultracapacitor Hybrid Energy Storage System. *IEEE Trans. Transp. Electrification* **2015**, *1*, 223–231. [[CrossRef](#)]
66. Wang, C.; Nehrir, M.H. Power Management of a Stand-Alone Wind/Photovoltaic/Fuel Cell Energy System. *IEEE Trans. Energy Convers.* **2008**, *23*, 957–967. [[CrossRef](#)]

Publisher's Note: MDPI stays neutral with regard to jurisdictional claims in published maps and institutional affiliations.



© 2020 by the authors. Licensee MDPI, Basel, Switzerland. This article is an open access article distributed under the terms and conditions of the Creative Commons Attribution (CC BY) license (<http://creativecommons.org/licenses/by/4.0/>).